

Surface Characteristics and Flexural Strength of Porous-Surface Designed Zirconia Manufactured via Stereolithography

Quanquan Ma DDS¹  | Qian Ding DDS^{1,2} | Lei Zhang DDS¹ | Yuchun Sun DDS^{3,4} | Qiufei Xie DDS¹

¹Department of Prosthodontics, Peking University School and Hospital of Stomatology & National Center of Stomatology & National Clinical Research Center for Oral Diseases & National Engineering Laboratory for Digital and Material Technology of Stomatology & Beijing Key Laboratory of Digital Stomatology & Research Center of Engineering and Technology for Computerized Dentistry Ministry of Health & NMPA Key Laboratory for Dental Materials, Beijing, China

²Foshan (Southern China) Institute for New Materials, Guangdong, China

³Center of Digital Dentistry, Peking University School and Hospital of Stomatology, Beijing, China

⁴National Engineering Laboratory for Digital and Material Technology of Stomatology, Research Center of Engineering and Technology for Digital Dentistry, Beijing, China

Correspondence

Lei Zhang, DDS, Department of Prosthodontics, Peking University School and Hospital of Stomatology; No. 22, Zhongguancun South Avenue, Haidian District, Beijing, 100081, PR China. E-mail: drzhanglei@yeah.net

Authors Quanquan Ma and Qian Ding contributed equally to this work.

Funding information

Guangdong Basic and Applied Basic Research Foundation, Grant/Award Number: 2019A1515110889; Capital Health Research and Development of Special Fund, Grant/Award Number: 2020-2-4104; Natural Science Foundation of Beijing Municipality, Grant/Award Number: 7192233

Abstract

Purpose: To design and fabricate zirconia bars with porous surfaces using stereolithography and evaluate their surface characteristics and flexural strengths.

Materials and Methods: Five groups of zirconia bars (20 mm × 4 mm × 2 mm) with interconnected porous surfaces were designed and manufactured: (i) 400- μ m pore size and 50% porosity (D400-P50 group), (ii) 400- μ m pore size and 30% porosity (D400-P30 group), (iii) 200- μ m pore size and 50% porosity (D200-P50 group), (iv) 200- μ m pore size and 30% porosity (D200-P30 group), and (v) 100- μ m pore size and 30% porosity (D100-P30 group). Zirconia bars without a porous surface (NP) were used as controls. The surface topographies and pore structures were investigated using scanning electron microscopy and three-dimensional laser microscopy. The printed porosity was calculated using the Archimedes method. Fifteen specimens from each group were subjected to a three-point bending test according to the ISO 6872:2015 standard. A Weibull analysis was performed, and the fractured surfaces were examined using scanning electron microscopy.

Results: Zirconia bars with porous surfaces were designed and successfully manufactured. The designed pore size, porosity, and shape of the printed pores were approximately achieved for all the porous surfaces. The flexural strength of the control group was significantly higher than those of the groups with porous surfaces ($p < 0.001$). For the same porosity, groups with a pore size of 400 μ m exhibited a lower flexural strength than the other groups ($p < 0.001$). Additionally, for the same pore-size design, the flexural strengths of group D400-P50 and D400-P30 exhibited no significant differences ($p = 0.150$), while the flexural strengths of D200-P30 were significantly higher than that of the D200-P50 group ($p = 0.043$). The control group and D400-P50 group had higher Weibull moduli than the other groups. The fractography of the specimens with porous surfaces indicated more than one crack origin, mainly owing to defects, including pores and cracks.

Conclusion: Zirconia bars with porous surfaces were successfully designed and fabricated using the stereolithography technique. Although porous surfaces may be advantageous for osteogenesis, the porous-surface design can reduce the flexural strength of the printed zirconia bars. By reducing the pore size, controlling the porosity, and improving the printing accuracy, a higher strength can be achieved.

KEYWORDS

Additive manufacture, flexural strength, porous surface, stereolithography, zirconia

Yttria-stabilized tetragonal zirconia polycrystal (Y-TZP)—a high-strength zirconia ceramic—has become an attractive material for dental implants.^{1–4} The surface microstructure of zirconia implants may be key to improving the osseointegration ability.⁵ Most previous works claim that porous surface with pore sizes between 100 and 400 μm and porosity higher than 30% are favorable for osteointegration.^{6,7}

Three-dimensional (3D)-printing, as a method of a 3D object creation through layer-by-layer additive manufacturing, has been widely investigated because of its potential in ceramic processing.^{8,9} Stereolithography (SLA), in which an object is fabricated via point-by-point polymerization of a photocuring material using an ultraviolet laser, is one of the most commonly used techniques.^{10,11} With suitable ceramic slurry, appropriate laser parameters and sintering process,^{12–15} it can provide zirconia features with high precision and good surface quality.^{14,16–20} Therefore, it was expected that this technique can be used to create a dental implant with a complex microstructure, such as a porous surface with a controlled pore size and porosity, which cannot be achieved with conventional techniques.^{21,22} Metal dental implants with porous surfaces and dense cores were recently reported to have the advantages of weakening the stress-shielding effect on the surrounding bones and improving osseointegration with long-term stability.^{23–25} However, zirconia with a porous surface and dense core has not been reported.

Dental restorations require adequate flexural strength to ensure they are permissible for clinical use and have enough durability under occlusal forces. The flexural strength of SLA-fabricated zirconia ceramics is closely related to the ceramic suspension, processing parameters, phase transformation, density, and internal and surface defects.^{9,26–28} The effects of the porous design on the mechanical properties of zirconia components remain unclear.

The objectives of this study were to design zirconia bars with porous surfaces and dense bases of different pore sizes and porosities using the SLA technique and to evaluate their surface characteristics and flexural strengths. The null hypothesis tested was that the porous surface, pore size, and porosity did not affect the flexural strength of zirconia.

MATERIALS AND METHODS

Design and fabrication of zirconia specimens

Five groups were designed according to different pore size and porosity: (i) 400- μm pore size and 50% porosity (D400-P50 group), (ii) 400- μm pore size and 30% porosity (D400-P30 group), (iii) 200- μm pore size and 50% porosity (D200-P50 group), (iv) 200- μm pore size and 30% porosity (D200-P30 group), and (v) 100- μm pore size and 30% porosity (D100-P30 group).

The design process for the porous surface is shown in Figure 1. First, a pore cell unit with porosity of 50% (Fig 1a) and 30% (Fig 1b) was created by Boolean operation respect-

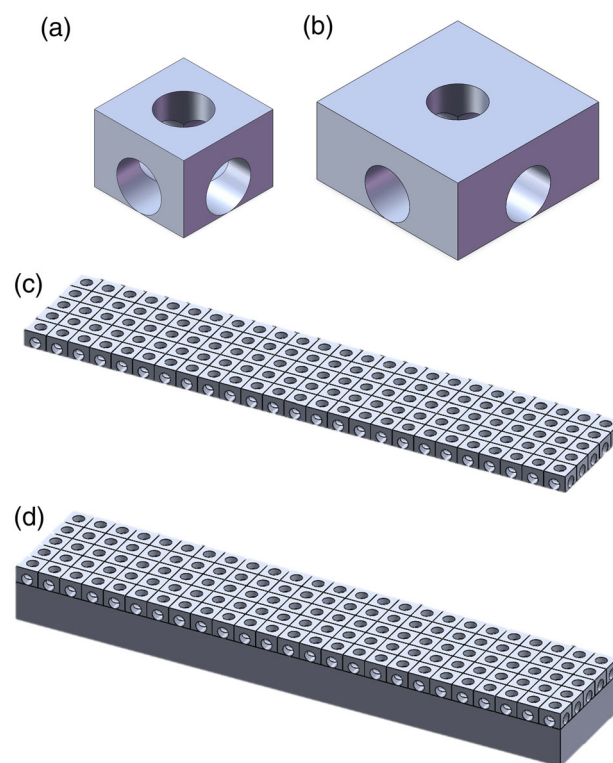


FIGURE 1 The design process of porous surface. (a) Pore cell unit for the volume fraction of 50%; (b) pore cell unit for the volume fraction of 30%; (c) tiling the pore cells to form a porous layer; and (d) adding a cuboid beneath the porous layer to obtain zirconia bars.

tively. Afterwards a porous layer with a length of 20 mm and width of 4 mm was formed by tiling the pore cells from the center to the periphery (Fig 1c). Then, a cuboid was added beneath the porous layer to obtain zirconia bars of the same size of 20 mm \times 4 mm \times 2 mm (Fig 1d). Finally, the models were processed using Materialize Magics 22 software (Materialize, Leuven, Belgium).

All zirconia bars were fabricated using a zirconia slurry provided by PORIMY via SLA printer (CSL-100; PORIMY Co., Kunshan, China). It contained of 49 vol% Y-TZP particles and photosensitive acrylic resin mixture. To eliminate the influence of scattering effect on the porous structure,^{12,29} a boundary compensation of 50 μm was applied.³⁰ After the specimens were printed, the uncured slurry on the surface and inside the pores was cleaned by air compressor. Subsequently, the green bodies were converted into zirconia components via organic burnout at 350°C to 550°C for 22 hours followed by sintering process at 1500°C for 2 hours in a sintering furnace (KSL-1700X, MTI Co., Hefei, China). The whole heat treatment lasts for 52 hours.¹⁷ As a control (NP) group, zirconia bars without porous surfaces were manufactured using the same processes.

Surface measurements

The pore diameters, surface roughness of the NP group and flat surface between the pores were measured using a 3D

laser microscope (VK-9700K, Keyence Co., Osaka, Japan). Additionally, the shape and distribution of printed pores were examined using a stereoscopic microscope (SZX7, OLYMPUS, Tokyo, Japan), while the surface microstructures such as grain arrangement and surface defects of the specimens were examined using scanning electron microscopy (SEM; JSM-6010LA, JEOL, Tokyo, Japan).

Density and porosity measurements

The density (ρ) of the specimens ($n = 3$) was measured using the Archimedes method according to the ASTM C373-18 standard,^{20,31,32} and the porosity of the porous layer was calculated by converting the overall porosity into the layer thickness.

X-ray diffraction (XRD) measurements

Three specimens from each group were analyzed using an X-ray diffractometer (D/max 2500, Rigaku, Japan) and the contents of monoclinic phase were calculated.³³

Flexural strength (σ) measurements, Weibull analysis, and fractography

Fifteen specimens from each group were subjected to a three-point bending test, according to the ISO 6872:2015 standard.³⁴ The specimens were loaded on a universal testing machine (AGS-X, SHIMADZU, Kyoto, Japan) with a crosshead speed of 1 mm/min and a loading span of 16 mm until failure. Then the structural reliability of each group was assessed via a Weibull distribution analysis of the flexural-strength data. The Weibull modulus m and characteristic strength σ_0 (strength value at 63.21% failure probability) were calculated at a 95% confidence interval in the software (MATLAB R2014a, MathWorks, Natick, MA). The crack origins and fractography characteristics were investigated via SEM.^{35–37}

Statistical analysis

Statistical analyses were performed using SPSS Statistics 26.0 (IBM, Chicago, IL). The mean pore size and porosity were compared with the design values using a one-sample t-test. The surface-roughness values were compared among the groups using a one-way analysis of variance, and an LSD test was performed to evaluate the differences between the two groups. The flexural strength exhibited heterogeneity of variance; thus, the statistical differences in flexural strengths were detected by Kruskal-Wallis and pairwise comparisons. The significance level for the comparisons was set as $p < 0.05$.

RESULTS

Surface observation and surface roughness

Zirconia bars with porous surfaces were successfully manufactured using SLA. Under stereomicroscopy and SEM, the printed pores were uniformly distributed, with round, regular, and consistent shapes (Fig 2). SEM revealed that at a high magnification, all the tested specimens exhibited a compact grain arrangement. The surface around the pores had inferior quality to that between the pores, appearing rougher and more irregular.

The mean values of surface roughness were showed in Table 1. Except for the D400-P30 group ($p = 0.014$), the roughness of the surface between the pores for other groups was not significantly different from that for the NP group ($p > 0.05$).

Density, pore-size, and porosity measurements

The calculated density of an SLA-printed zirconia specimen without a porous surface was 6.01 g/cm^3 , which was 98.8% of the theoretical density of zirconia (6.08 g/cm^3). Table 2 presents the pore sizes and porosities for the five groups with porous surfaces. The pore size of the D400-P50 was significantly smaller than the design value ($p = 0.003$). For the D100-P30 and D400-P50, the porosity of the porous layer was significantly lower than the design value ($p = 0.003$ and $p = 0.008$). The pore parameters of the other groups were similar to the corresponding design values ($p > 0.05$).

Phase transformation

The XRD patterns exhibited no obvious monoclinic phase peak for any of the groups (Fig 3). The calculated surface monoclinic phase content was 3.99%, 6.31%, 5.75%, 7.67%, 5.78%, and 4.58% for the NP, D400-P50, D400-P30, D200-P50, D200-P30, and D100-P30 groups, respectively.

Flexural strength measurements and Weibull characteristics

The flexural strengths and Weibull characteristics are presented in Table 3. All five porous-surface groups had significantly lower flexural strengths than the NP group ($p < 0.001$). Zirconia bars with smaller pore sizes exhibited higher flexural strengths. For the same porosity, the flexural strength of the D200-P50 group was significantly higher than that of the D400-P50 group ($p = 0.002$), and the flexural strength of the D100-P30 group was significantly higher than that of the D400-P30 groups ($p < 0.001$). For the same pore-size, the flexural strengths of group D400-P50 and D400-P30 exhibited no significant differences ($p > 0.05$) but the flexural strength of group D200-P30 was significantly higher than

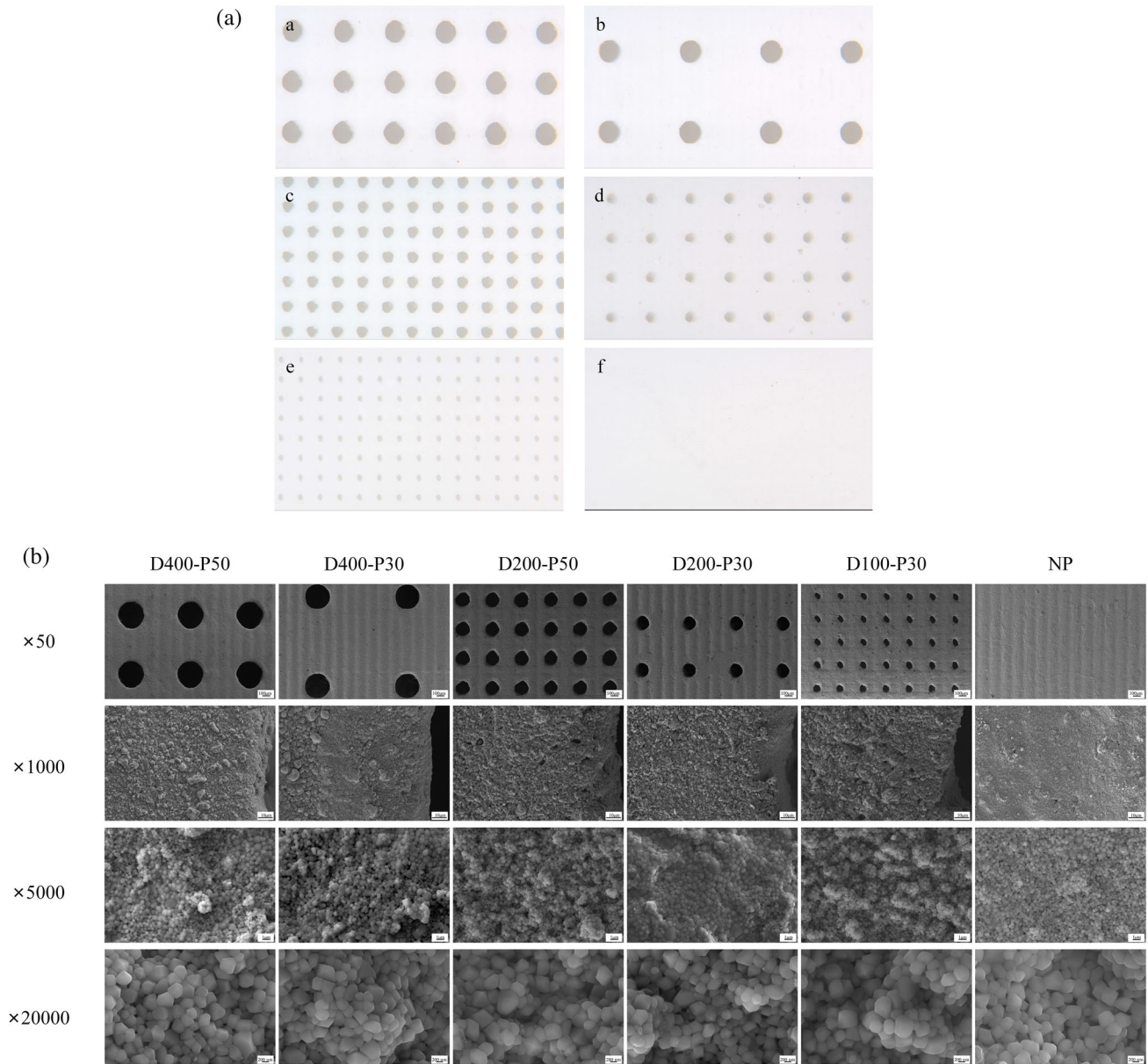


FIGURE 2 (A) Surface morphologies of SLA-manufactured zirconia bars in stereomicroscopy. (a) D400-P50 group; (b) D400-P30 group; (c) D200-P50 group; (d) D200-P30 group; (e) D100-P30 group; and (f) NP group. (B) Surface microstructures of SLA-manufactured zirconia bars in scanning electron microscopy.

that of D200-P50 ($p < 0.05$). The Weibull analysis (Fig 4) exhibited a higher Weibull modulus for the NP (12.82) and D400-P50 (19.83) groups than for the other groups.

Fractographic analysis

Figure 5a shows SEM images of the fractured surfaces for the six groups after the three-point bending test. The fractured surfaces of the specimens of the NP group exhibited classic hackle lines radiating from the crack origins at the defects located on the surface or beneath the surface on the tensile-stress side, where the processing flaws were observed. However, for the specimens with porous surfaces, the frac-

ture patterns were complex. More than one crack origins were observed owing to flaws including pores, agglomerations, cracks, and delamination (Fig 5b), which were mainly located at the bottoms or edges of the pores or inside the channels connecting adjacent pores. Starting from multiple crack origins, the crack propagation paths were disturbed or interlaced.

DISCUSSION

In this study, gradient zirconia with a porous surface was designed through forward modeling technology and fabricated via the SLA technique with acceptable precision.

TABLE 1 The surface roughness of two groups with no surface modification

| Groups | Ra (μm) | Rz (μm) | Rq (μm) |
|----------|--------------|-------------|-------------|
| NP | 0.60 ± 0.13 | 4.11 ± 0.84 | 0.75 ± 0.17 |
| D400-P50 | 0.67 ± 0.09 | 4.37 ± 0.64 | 0.83 ± 0.11 |
| D400-P30 | 0.70 ± 0.13* | 4.37 ± 1.05 | 0.87 ± 0.17 |
| D200-P50 | 0.64 ± 0.09 | 4.14 ± 0.64 | 0.79 ± 0.12 |
| D200-P30 | 0.68 ± 0.11 | 4.43 ± 1.05 | 0.99 ± 0.71 |
| D100-P30 | 0.63 ± 0.14 | 4.05 ± 1.05 | 0.78 ± 0.16 |

*P < 0.05 compared to the NP group.

TABLE 2 The printed pore size, interval, and porosity of groups with porous surface

| Groups | Pore size (μm) | Porosity (%) | Porosity of porous layer (%) |
|----------|-----------------|----------------|------------------------------|
| D400-P50 | 364.75 ± 3.77** | 13.93 ± 0.44** | 43.73** |
| D400-P30 | 386.57 ± 11.45 | 10.43 ± 0.30 | 31.49 |
| D200-P50 | 196.75 ± 1.44 | 7.28 ± 0.14 | 48.07 |
| D200-P30 | 197.70 ± 1.91 | 4.49 ± 0.05 | 28.29 |
| D100-P30 | 94.34 ± 2.28 | 3.31 ± 0.19 | 20.65** |

**P < 0.01 compared to the corresponding designed value.

The results indicated that although the porous surface layer may be advantageous for osteogenesis, it could significantly reduce the flexural strength of SLA fabricated zirconia. The larger the pore size and the higher the porosity, the lower the flexural strength. Thus, the null hypothesis was rejected.

The printing accuracy of zirconia is closely related to each stage of the SLA process. In the light-curing molding stage, due to the different refractive indexes between resin and zirconia materials, light scattering can occur on the surface of the ceramic particles within the slurry and cause a broadening of the cured area and a reduction in the depth, resulting in a larger amount of surface surrounding the inner opening, reducing the pore size, and increasing the wall thickness.^{12,29} The D400-P50 group exhibited a significantly smaller pore size and lower porosity than the design, which can be partly explained by the light-scattering effects. In the sintering stage, ceramic shrinkage after heat treatment and improper degreasing sintering may lead to cracking and deformation of the specimens.¹³ The D100-P30 group exhibited a significantly lower porosity than the design, which was mainly attributed to the difficulty of cleaning post-treatment due to the small pore size. Controlling the content of the ceramics in the slurry,¹⁵ adjusting the laser intensity and layer thickness, setting adequate compensation for the sintering

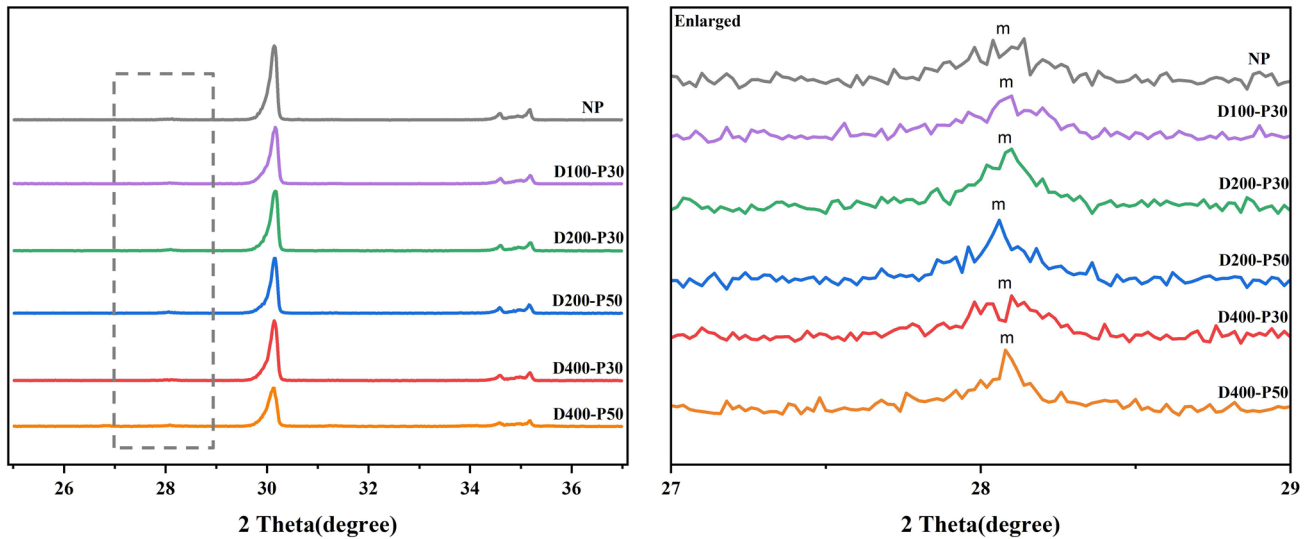


FIGURE 3 X-ray diffraction spectra of the zirconia bars.

TABLE 3 Flexural strengths and Weibull modulus

| Group | Flexural strength (MPa) (σ _c) | Characteristic strength (MPa) (σ ₀) | 95% CI | Weibull modulus (m) | 95% CI |
|----------|---|---|--------------------|---------------------|----------------|
| NP | 1039.76 ± 107.98 | 1084.40 | [1040.40, 1130.30] | 12.82 | [8.50, 19.33] |
| D400-P50 | 214.03 ± 12.18 | 203.79 | [198.38, 209.34] | 19.83 | [13.13, 29.95] |
| D400-P30 | 217.27 ± 28.84 | 227.42 | [217.62, 237.67] | 11.91 | [7.84, 18.09] |
| D200-P50 | 255.01 ± 30.89 | 268.99 | [250.86, 288.43] | 7.73 | [5.47, 10.91] |
| D200-P30 | 311.84 ± 67.58 | 336.41 | [311.36, 363.47] | 6.60 | [4.31, 10.11] |
| D100-P30 | 348.91 ± 60.15 | 374.05 | [344.60, 406.00] | 6.54 | [4.43, 9.66] |

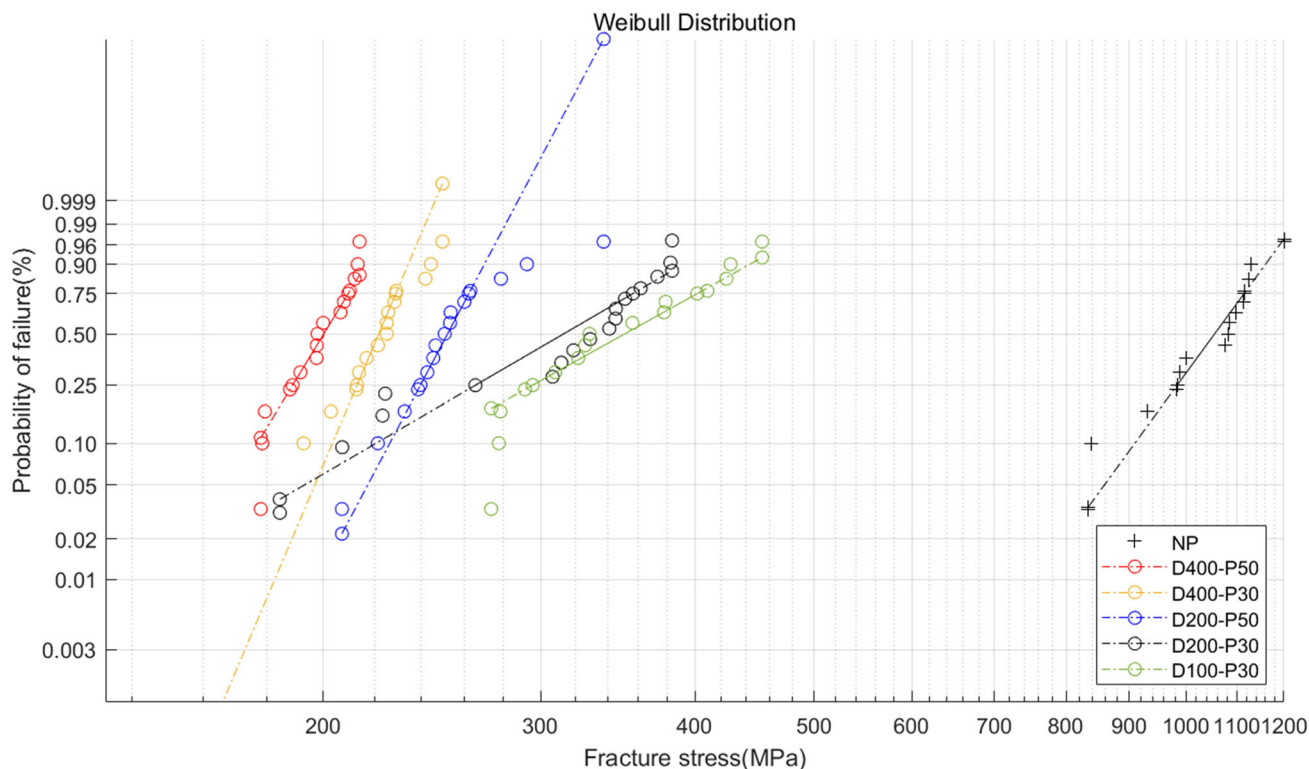


FIGURE 4 Weibull distribution of the SLA-printed zirconia bars.

shrinkage,³⁰ and optimizing the post-treatment process may help to reduce the deformation and dimension changes of 3D-printed ceramics and increase the dimensional accuracy, mechanical strength, and density.^{12,13}

In this study, the NP group exhibited a flexural strength of (1039.76 ± 107.98) MPa, which is higher than or similar to those reported in related previous works,^{9,11,19} indicating that the zirconia slurry and processing parameters used in this study are appropriate for 3D printing zirconia. The significantly reduced flexural strengths of the porous surface designed zirconia in this study were mainly attributed to the significant growth of surface and internal defects accompanied by the porous layer. Defects such as pores, cracks, inclusions, and delamination, which were observed in the SEM images of the cross-sections and surfaces of the specimens, acted as stress concentrators during crack nucleation, and then the cracks propagated, leading to fracture. Owing to the viscosity of the zirconia slurry, impurities in the air can adhere to the slurry, and air bubbles can be trapped during the printing process, resulting in inclusions and pores.³⁶ In addition, defects caused by the de-binding of polymers from the green parts during the sintering process may become visible as cracks.³⁶ Besides, because of the layered forming process, insufficient adhesion between two adjacent layers could cause defects between the layers, which is called delamination.^{37,10} The fractography results in this study revealed that compared with the NP group, the specimens with porous surfaces exhibited more internal pores, inclusions, and cracks in or near the porous layer, which were mainly located at the bottoms

or edges of the pores or inside the connecting channels. It can be deduced that the porous-surface design may affect the adhesion between layers, and the significant density difference between the porous layer and the dense base may lead to anisotropic shrinkage during the sintering process, resulting in cracks at the interface. Therefore, the results indicated that the porous surface structure can degrade the printing quality and increase the number of defects, reducing the flexural strength of the zirconia. In order to reduce the defects, the SLA process can be optimized by using different proportions of the slurry and laser parameters to produce different structures, and improving the printing and sintering environment.²⁸

Meanwhile, the porous surface structure itself can be regarded as a macroscopic surface defect in materials. It has been reported that the size and shape regularity of surface defects are the main factors that impair the fracture strength, and an increase in the pore size can reduce the stiffness and strength of the material.²⁵ In this study, significantly higher flexural strengths were observed for zirconia specimens with smaller pore sizes. This may be due to the stress concentration of the large pores, from which the cracks tended to originate, rather than other randomly allocated defects. Additionally, the specimens with larger pore size also had thicker porous layer, which could result in more internal and surface defects than those with smaller pore size. Although high porosity may facilitate cell spreading and osteogenic differentiation, it has been reported to reduce the flexural strength and flexural modulus of 3D-printed zirconia significantly compared

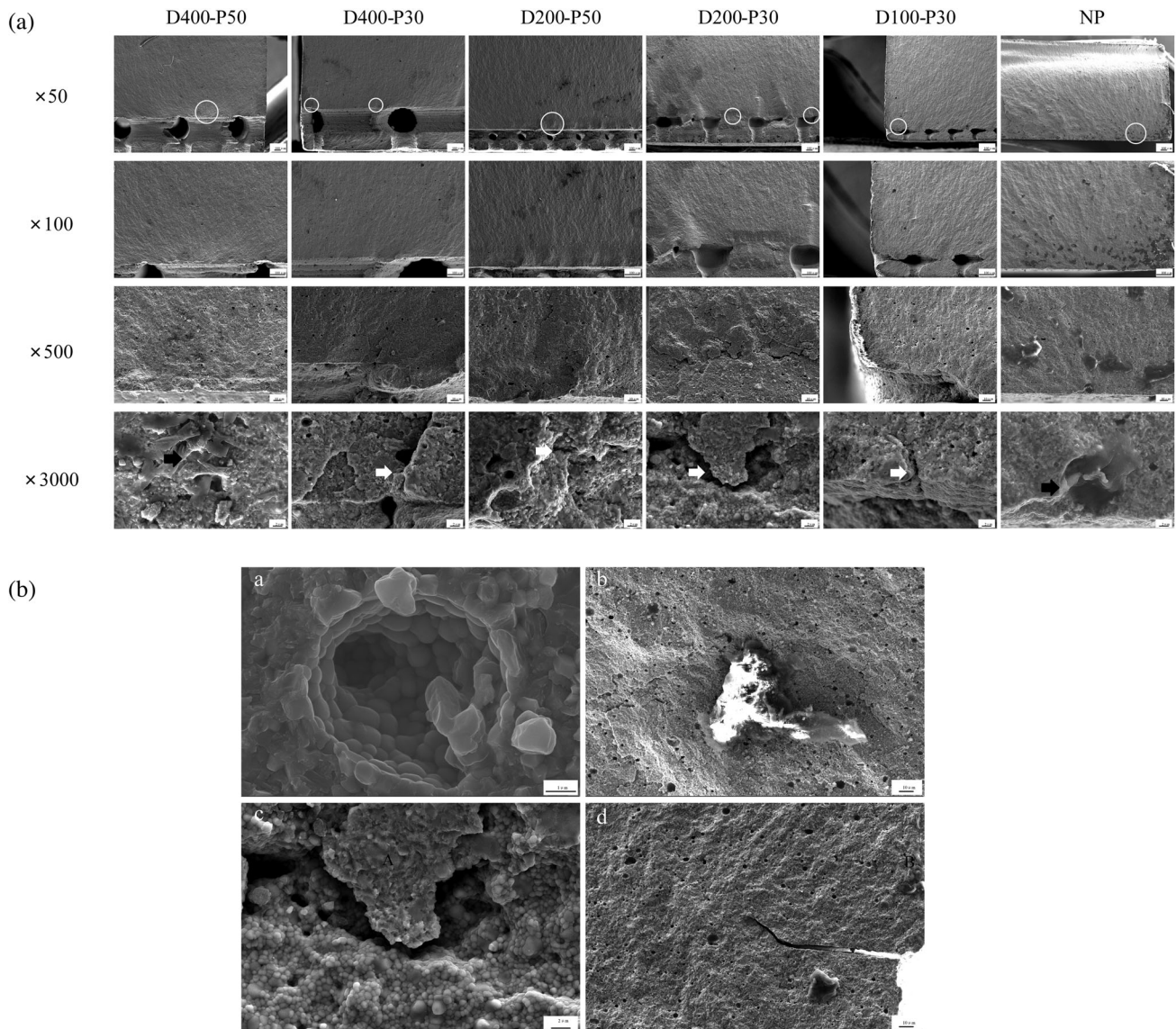


FIGURE 5 (A) SEM photographs of the fractured surfaces after three-point bending tests; the white circles show the crack origins, the white arrows show the cracks, and the black arrow shows a pore. (B) SEM observations of fractured surfaces, (a) pore; (b) agglomeration; (c) cracks; and (d) delamination.

with milled and 3D-printed low-porosity zirconia. And zirconia with a porosity of 40% exhibited a flexural strength of only (48.09 ± 8.95) MPa.³⁸ In this study, the flexural strength in group D200-P50 is significantly lower than that of D200-P30 group. But there was no significant difference between the flexural strengths of D400-P30 and D400-P50 groups, which may be explained by that the surface defects in 400- μ m pore-size groups, with larger pore size and thicker porous layer than 200- μ m groups. These results suggest that reducing the pore size, increasing the thickness of the base as well as controlling the porosity can be beneficial for increasing the flexural strength of zirconia with porous surfaces.

Additive manufacturing technology represents a promising alternative to conventional machining procedures, with advantages such as the ability to manufacture specimens with micro-scale and complex geometries, reduced material waste and energy consumption, and the ability to form structures

with multiple materials.^{8,20} This allows the mass production of customized dental products with control over both surface and internal structures. However, according to the results of this study, further developments are needed to improve the mechanical properties and printing accuracy of 3D-printed zirconia with porous surface for dental applications. Further studies should be conducted on the fatigue characteristics and biological properties of zirconia with porous surfaces. Additionally, whether the mechanical properties of porous zirconia are affected by physical and chemical environmental factors requires further investigation.

CONCLUSION

Porous-surface zirconia bars were successfully designed and fabricated using SLA. Although porous surfaces may have

advantages for osteogenesis, attention should be paid to the significant reduction in the flexural strength of zirconia with porous surfaces. By reducing the pore size, controlling the porosity, and increasing the printing accuracy, a higher strength can be achieved.

ACKNOWLEDGEMENTS

This work was supported by Beijing Natural Science Foundation (grant number: 7192233), Capital Health Research and Development of Special Fund (grant number: 2020-2-4104), and Guangdong Basic and Applied Basic Research Foundation (2019A1515110889).

CONFLICT OF INTEREST

There is no conflict of interest.

ORCID

Quanquan Ma DDS  <https://orcid.org/0000-0001-6650-4007>

REFERENCES

- Ding Q, Zhang R, Zhang L, et al. Effects of different microstructured surfaces on the osseointegration of CAD/CAM zirconia dental implants: an experimental study in rabbits. *Int J Oral Maxillofac Implants* 2020;35:1113-1121.
- Kubasiewicz-Ross P, Hadzik J, Dominiak M. Osseointegration of zirconia implants with 3 varying surface textures and a titanium implant: a histological and micro-CT study. *Adv Clin Exp Med* 2018;27:1173-1179.
- ArRejaie AS, Al-Hamdan RS, Basunbul GI, et al. Clinical performance of one-piece zirconia dental implants: a systematic review. *J Investig Clin Dent* 2019;10:e12384-e12390.
- Cionca N, Hashim D, Mombelli A. Zirconia dental implants: where are we now, and where are we heading? *Periodontol* 2000 2017;73:241-258.
- Hadjicharalambous C, Prymak O, Loza K, et al. Effect of porosity of alumina and zirconia ceramics toward Pre-Osteoblast response. *Front Bioeng Biotechnol* 2015;3:175.
- Zaharin HA, Abdul RA, Azam FI, et al. Effect of unit cell type and pore size on porosity and mechanical behavior of additively manufactured Ti6Al4V scaffolds. *Materials (Basel)* 2018;11:2402.
- Liu Y, Rath B, Tingart M, et al. Role of implants surface modification in osseointegration: a systematic review. *J Biomed Mater Res* 2020;108:470-484.
- Osman RB, van der Veen AJ, Huiberts D, et al. 3D-printing zirconia implants. a dream or a reality? An in-vitro study evaluating the dimensional accuracy, surface topography and mechanical properties of printed zirconia implant and discs. *J Mech Behav Biomed Mater* 2017;75:521-528.
- Revilla-Leon M, Meyer MJ, Zandinejad A, et al. Additive manufacturing technologies for processing zirconia in dental applications. *Int J Comput Dent* 2020;23:27-37.
- Xiang D, Xu Y, Bai W, et al. Dental zirconia fabricated by stereolithography: accuracy, translucency and mechanical properties in different build orientations. *Ceram Int* 2021;47:28837-28847.
- Revilla-Leon M, Al-Haj HN, Ceballos L, et al. Flexural strength and Weibull characteristics of stereolithography additive manufactured versus milled zirconia. *J Prosthet Dent* 2021;125:685-690.
- Conti L, Bienenstein D, Borlaf M, et al. Effects of the layer height and exposure energy on the lateral resolution of zirconia parts printed by lithography-based additive manufacturing. *Materials (Basel)* 2020;13:1317.
- Li H, Song L, Sun J, et al. Stereolithography-fabricated zirconia dental prostheses: concerns based on clinical requirements. *Adv Appl Ceram* 2020;119:236-243.
- Wang W, Sun J. Dimensional accuracy and clinical adaptation of ceramic crowns fabricated with the stereolithography technique. *J Prosthet Dent* 2021;125:657-663.
- Felzmann R, Gruber S, Mitterramskogler G, et al. Lithography-based additive manufacturing of cellular ceramic structures. *Adv Eng Mater* 2012;14:1052-1058.
- Li R, Chen H, Wang Y, et al. Performance of stereolithography and milling in fabricating monolithic zirconia crowns with different finish line designs. *J Mech Behav Biomed Mater* 2021;115:104255-104255.
- Li R, Wang Y, Hu M, et al. Strength and adaptation of stereolithography-fabricated zirconia dental crowns: an in vitro study. *Int J Prosthodont* 2019;32:439-443.
- Li R, Xu T, Wang Y, et al. Accuracy of zirconia crowns manufactured by stereolithography with an occlusal full-supporting structure: an in vitro study. *J Prosthet Dent* 2022. In press. <https://doi.org/10.1016/j.prosdent.2022.01.015>
- Xing H, Zou B, Li S, et al. Study on surface quality, precision and mechanical properties of 3D printed ZrO₂ ceramic components by laser scanning stereolithography. *Ceram Int* 2017;43:16340-16347.
- Dehurtevent M, Robberecht L, Hornez JC, et al. Stereolithography: a new method for processing dental ceramics by additive computer-aided manufacturing. *Dent Mater* 2017;33:477-485.
- Ohji T, Fukushima M. Macro-porous ceramics: processing and properties. *Int Mater Rev* 2013;57:115-131.
- Roedel S, Mesquita-Guimaraes J, Souza J, et al. Production and characterization of zirconia structures with a porous surface. *Mater Sci Eng C Mater Biol Appl* 2019;101:264-273.
- Sadollah A, Bahreininejad A. Optimum gradient material for a functionally graded dental implant using metaheuristic algorithms. *J Mech Behav Biomed Mater* 2011;4:1384-1395.
- Asgharzadeh SH, Ayatollahi MR, Asnafi A. To reduce the maximum stress and the stress shielding effect around a dental implant-bone interface using radial functionally graded biomaterials. *Comput Methods Biomech Biomed Engin* 2017;20:750-759.
- Kelly CN, Evans NT, Irvin CW, et al. The effect of surface topography and porosity on the tensile fatigue of 3D printed Ti-6Al-4V fabricated by selective laser melting. *Mater Sci Eng C Mater Biol Appl* 2019;98:726-736.
- Li X, Zhong H, Zhang J, et al. Dispersion and properties of zirconia suspensions for stereolithography. *Int J Appl Ceram Tec* 2020;17:239-247.
- Wang B, Arab A, Xie J, et al. The Influence of microstructure on the flexural properties of 3D printed zirconia part via digital light processing technology. *Materials (Basel)* 2022;15:1602.
- Galante R, Figueiredo-Pina CG, Serro AP. Additive manufacturing of ceramics for dental applications: a review. *Dent Mater* 2019;35:825-846.
- Mitterramskogler G, Gmeiner R, Felzmann R, et al. Light curing strategies for lithography-based additive manufacturing of customized ceramics. *Addit Manuf* 2014;1-4:110-118.
- Wang X, Zou B, Li L, et al. Manufacturing of a ceramic groove part based on additive and subtractive technologies. *Ceram Int* 2020;47:740-747.
- Lu Y, Mei Z, Zhang J, et al. Flexural strength and Weibull analysis of Y-TZP fabricated by stereolithographic additive manufacturing and subtractive manufacturing. *J Eur Ceram Soc* 2020;40:826-834.
- American Society of Testing Materials: ASTM C373-18. Standard test methods for determination of water absorption and associated properties by vacuum method for pressed ceramic tiles and glass tiles and boil method for extruded ceramic tiles and non-tile fired ceramic white-ware products. West Conshohocken, PA, ASTM International; 2018. <https://www.astm.org/c0373-18.html>
- Toraya H, Yoshimura M, Somiya S. Calibration curve for quantitative analysis of the monoclinic-tetragonal ZrO₂ system by X-ray diffraction. *J Am Ceram Soc* 1984;67:C119-C121.

34. International Organization for Standardization: ISO 6872:2015. Dentistry — Ceramic Materials. Geneva, International Organization for Standardization; 2015. <https://www.iso.org/standard/59936.html>
35. Scherrer SS, Lohbauer U, Bona AD, et al. ADM guidance—ceramics: guidance to the use of fractography in failure analysis of brittle materials. *Dent Mater* 2017;33:599-620.
36. Harrer W, Schwentenwein M, Lube T, et al. Fractography of zirconia-specimens made using additive manufacturing (LCM) technology. *J Eur Ceram Soc* 2017;37:4331-4338.
37. Jang KJ, Kang JH, Fisher JG, et al. Effect of the volume fraction of zirconia suspensions on the microstructure and physical properties of products produced by additive manufacturing. *Dent Mater* 2019;35:e97-e106.
38. Zandinejad A, Das O, Barmak AB, et al. The flexural strength and flexural modulus of stereolithography additively manufactured zirconia with different porosities. *J Prosthodont* 2022;31:434-440. <https://doi.org/10.1111/jopr.13430>

How to cite this article: Ma Q, Ding Q, Zhang L, Sun Y, Xie Q. Surface Characteristics and Flexural Strength of Porous-Surface Designed Zirconia Manufactured via Stereolithography. *J Prosthodont*. 2023;32:e81–e89. <https://doi.org/10.1111/jopr.13565>